

## Local Noise Spectroscopy of Wigner Crystals in Two-Dimensional Materials

Pavel E. Dolgirev<sup>1,\*</sup>, Ilya Esterlis<sup>2,1,\*</sup>, Alexander A. Zibrov,<sup>1</sup> Mikhail D. Lukin,<sup>1</sup>  
Thierry Giamarchi<sup>3</sup>, and Eugene Demler<sup>4</sup>

<sup>1</sup>*Department of Physics, Harvard University, Cambridge, Massachusetts 02138, USA*

<sup>2</sup>*Department of Physics, University of Wisconsin-Madison, Madison, Wisconsin 53706, USA*

<sup>3</sup>*Department of Quantum Matter Physics, University of Geneva, 24 quai Ernest-Ansermet, 1211 Geneva, Switzerland*

<sup>4</sup>*Institute for Theoretical Physics, ETH Zurich, 8093 Zurich, Switzerland*

 (Received 19 September 2023; revised 10 February 2024; accepted 14 May 2024; published 14 June 2024)

We propose local electromagnetic noise spectroscopy as a versatile and noninvasive tool to study Wigner crystal phases of strongly interacting two-dimensional electronic systems. In-plane imaging of the local noise is predicted to enable single-site resolution of the electron crystal when the sample-probe distance is less than the interelectron separation. At larger sample-probe distances, noise spectroscopy encodes information about the low-energy Wigner crystal phonons, including the dispersion of the transverse shear mode, the pinning resonance due to disorder, and optical modes emerging, for instance, in bilayer crystals. We discuss the potential utility of local noise probes in analyzing the rich set of phenomena expected to occur in the vicinity of the melting transition.

DOI: [10.1103/PhysRevLett.132.246504](https://doi.org/10.1103/PhysRevLett.132.246504)

Wigner crystal (WC) phases of the electron gas have been a subject of active research since their initial conception by Wigner many years ago [1]. Recently, a new generation of experiments providing compelling evidence of WC phases across a number of two-dimensional electron gas (2DEG) systems [2–6] have reinvigorated interest in the field for a number of reasons: (i) the experiments are in the degenerate regime  $T \ll E_F$  ( $E_F$  is the Fermi energy) and at zero perpendicular magnetic field; (ii) unexpected magnetism has been observed in the vicinity of the WC melting transition [4–6]; (iii) in transition metal dichalcogenide (TMD) systems, optical spectroscopy enabled direct measurement of the WC ordering wave vector [2]; and (iv) TMD bilayer WCs appear stable up to anomalously high electron densities and temperatures [3].

Despite both novel and improved experimental capabilities for clarifying the onset of crystallization, there remain few probes for characterizing salient properties of the WC phase [7]. These include the nano and mesoscale structure of the electron crystal, as well as properties of the low-energy WC phonons [9]. The necessity of experimental proposals is especially pressing in the TMD systems, for which many conventional measurements, such as transport, are not possible due to notorious challenges associated with large contact resistances [10,11].

In this Letter we propose local electromagnetic noise spectroscopy as a probe of WC states, and consider the conditions under which such measurements are within current experimental reach. We demonstrate that, owing to the large emergent length scale associated with the WC lattice constant, magnetic noise spectroscopy can be used to both map local charge properties at the WC lattice scale, as

well as long-wavelength properties of the WC phonons. We show that magnetic noise sensing is especially well-suited to probe a defining feature of the WC solid—the transverse shear mode. Other resonances unique to the crystal phase can also be observed, such as the “pinning resonance” due to disorder and optical modes in more complex crystals like bilayer WCs. Our proposal is in part inspired by developments in the field of “qubit” sensors, in which quantum impurities of various sorts are used to probe local electromagnetic fields and their associated fluctuations. Notable probes include nitrogen-vacancy and silicon-vacancy centers in diamond [12–27], hexagonal boron nitride defects [28–33], and stands for scanning near-field optical microscopy detectors [34,35], which can sense magnetic and/or electric fields [36–41].

We consider an atomic scale qubit probe brought near a 2D sample of interest and used to sense local magnetic fields. Fluctuating currents in the sample generate stray magnetic fields, which then affect the relaxation properties of the qubit [42]. These relaxation properties are directly related to the magnetic noise tensor

$$\mathcal{N}_{\alpha\beta}^B(\mathbf{r}_q, \omega) = \frac{1}{2} \int dt e^{i\omega t} \langle \{B_\alpha(\mathbf{r}_q, t), B_\beta(\mathbf{r}_q, 0)\} \rangle_T, \quad (1)$$

where  $\{.,.\}$  is the anticommutator,  $\langle \dots \rangle_T$  denotes the thermal expectation value,  $\mathbf{r}_q = (\mathbf{r}, z_q)$  is the position of the noise probe, and Greek indices  $\alpha, \beta$ , etc., denote Cartesian components. The Biot-Savart law further relates the magnetic field to currents via  $B_\alpha(\mathbf{q}, z) = (2\pi/qc)e^{-q|z|}\epsilon_{\alpha\beta\gamma}(iq_\beta - q\delta_{\beta z})j_\gamma(\mathbf{q}) \equiv K_{\alpha\gamma}(\mathbf{q}, z)j_\gamma(\mathbf{q})$ , with  $j_\alpha(\mathbf{q})$  the 2D current density in the sample. Here,  $\mathbf{q}$  is the in-plane wave vector,  $c$  is the speed of light, and  $\epsilon_{\alpha\beta\gamma}$  is the

Levi-Civita tensor [43]. Experimentally, one usually accesses  $\mathcal{N}_{\alpha\beta}^B$  via  $1/T_1$  relaxometry and/or  $1/T_2$  spin-echo-like measurements related to the noise via Fermi's golden rule. The dependence of the magnetic noise tensor on various physical parameters—such as temperature, frequency, qubit's position, electron density, etc.—allows one to characterize intrinsic correlations of the 2D material [18,45,46,60–64]. This has been demonstrated in a variety of systems, including hydrodynamic transport in 2D metals [45], 2D superconductors [63,64], and different magnetic phases and phase transitions [46,60,62].

The key idea of our work is based on the observation that the WC lattice constant, which is tuned by varying the electron density, can be made much larger than the underlying microscopic lattice scale of the 2D material. For instance, in TMDs the WC lattice constant varies in the range  $a \simeq 10\text{--}30$  nm [2,3]. This opens the possibility that a qubit probe can be brought closer to the 2D sample than the interelectron distance, allowing for spatial resolution of magnetic noise produced by individual electrons in the WC [65]. Magnetic noise in a WC is sourced primarily by charges oscillating about their equilibrium lattice sites, i.e., by local phonon fluctuations. In the regime  $z_q \lesssim a$ , the noise sensor effectively probes the local phonon density of states  $g(\omega)$ , with the noise directly on top of an electron being approximately given by [c.f., Eq. (4)],

$$\mathcal{N}^B(\omega) \sim \frac{Tne^2}{c^2m} g(\omega) \left( \sum_{\mathbf{G}} e^{-z_q G} \right)^2, \quad (2)$$

where  $\mathbf{G}$  are reciprocal lattice vectors of the WC and  $m$  is the effective electron mass. In TMD systems specifically, the noise will receive an enhancement owing to the relatively large melting temperatures (on the order of tens of K) and the relatively high electron densities ( $n \sim 10^{11}\text{--}10^{12}$  cm $^{-2}$ ). The magnitude of the density of states contribution depends on the ratio of the probe frequency to the plasma frequency,  $\omega_p^2 = 2\pi ne^2/ma$ , which is the characteristic phonon frequency scale in a WC. For WCs realized in TMD systems,  $\omega_p$  is on the order of a few THz. Typical resonant frequencies of atomlike solid-state defects, however, are in the GHz range, so we

expect  $\omega \ll \omega_p$ . The density of states then comes primarily from low-frequency transverse phonons,  $g(\omega) \approx \omega/2\pi v_s^2$ , where  $v_s$  is the sound speed (see also Ref. [66]). In this regime, we estimate the noise will be within the sensitivity of current sensors ( $\mathcal{N}^B \gtrsim 1$  pT $^2 \times$  Hz $^{-1}$ ) for a sample-probe distance on the order of a few nm. For probes with operating frequencies in the THz, such as tin-vacancy sensors [67] and SNOM detectors [68],  $g(\omega)$  would be larger and the sample-probe distance could be tens of nm. Additionally, nonlinear optics methods may be used to push the qubit operating regime to higher frequency [69,70]. Our estimates indicate that while single-site resolution (SSR) of the WC using noise spectroscopy is challenging, it nevertheless, can be within experimental reach. In what follows, we develop the general microscopic theory for electromagnetic noise from a WC. In addition to the SSR regime, we will also show that the noise allows one to study long-wavelength WC phonons when  $z_q \gtrsim a$ .

Deep in the WC, current fluctuations are generated by the time-varying polarization from fluctuating WC phonons. The phonon spectrum is described by the elastic potential energy  $U_{\text{el}} = \frac{1}{2} \sum_{\mathbf{q}} \sum_{\lambda} m \omega_{\lambda}^2(\mathbf{q}) |u_{\lambda}(\mathbf{q})|^2$ . Here,  $\lambda$  is the phonon mode index, which includes the transverse (shear) and longitudinal (compression) modes, as well as optical modes in crystals with more than one electron per unit cell (bilayer WCs);  $u_{\lambda}(\mathbf{q})$  are the associated phonon displacements with in-plane wave vector  $\mathbf{q}$ ; and the mode frequencies are  $\omega_{\lambda}(\mathbf{q})$ . These mode frequencies take into account both the Coulomb forces between electrons, as well as the effects of weak disorder—a point we will discuss below. The response properties of the WC are encoded in the phonon Green's function

$$D_{\alpha\beta}(\mathbf{q}, \omega) = -i \int_0^{\infty} dt e^{i\omega t} \langle [u_{\alpha}(\mathbf{q}, t), u_{\beta}(-\mathbf{q}, 0)] \rangle_T, \quad (3)$$

which can be directly related to the nonlocal optical conductivity of the WC [44,71].

The fluctuation-dissipation theorem and Bio-Savart law relate the magnetic noise tensor to the phonon Green's function [44]:

$$\mathcal{N}_{\alpha\beta}^B(\mathbf{r}, \omega) \approx 2Tne^2\omega \text{Im} \left[ \sum_{\mathbf{G}_1, \mathbf{G}_2} e^{i\mathbf{r} \cdot (\mathbf{G}_1 - \mathbf{G}_2)} \int_{\text{1BZ}} \frac{d^2\mathbf{q}}{(2\pi)^2} \mathcal{K}_{\alpha\gamma}(\mathbf{q} + \mathbf{G}_1, z_q) \mathcal{K}_{\beta\delta}(-\mathbf{q} - \mathbf{G}_2, z_q) D_{\gamma\delta}(\mathbf{q}, \omega) \right]. \quad (4)$$

Here, the  $\mathbf{q}$  integration is over the first Brillouin zone of the WC lattice,  $e$  is the electron charge, and we have assumed  $T \gg \hbar\omega$ . The exponential  $z$  dependence of  $\mathcal{K}_{\alpha\beta}$  implies that the qubit probe effectively averages over a spatial region with a size determined by  $z_q$  and, thus, one should distinguish two regimes:  $z_q \lesssim a$  and  $z_q \gtrsim a$ .

In the limit  $z_q \lesssim a$  (SSR regime), the contribution of nonzero  $\mathbf{G}$ 's, which determine the intraunit cell structure, is important. In this case, the largest contribution to the noise comes from positions  $\mathbf{r}$  near the WC lattice sites, where the oscillating phase factors in Eq. (4) go to one. Figure 1 illustrates the important characteristics of the noise in the

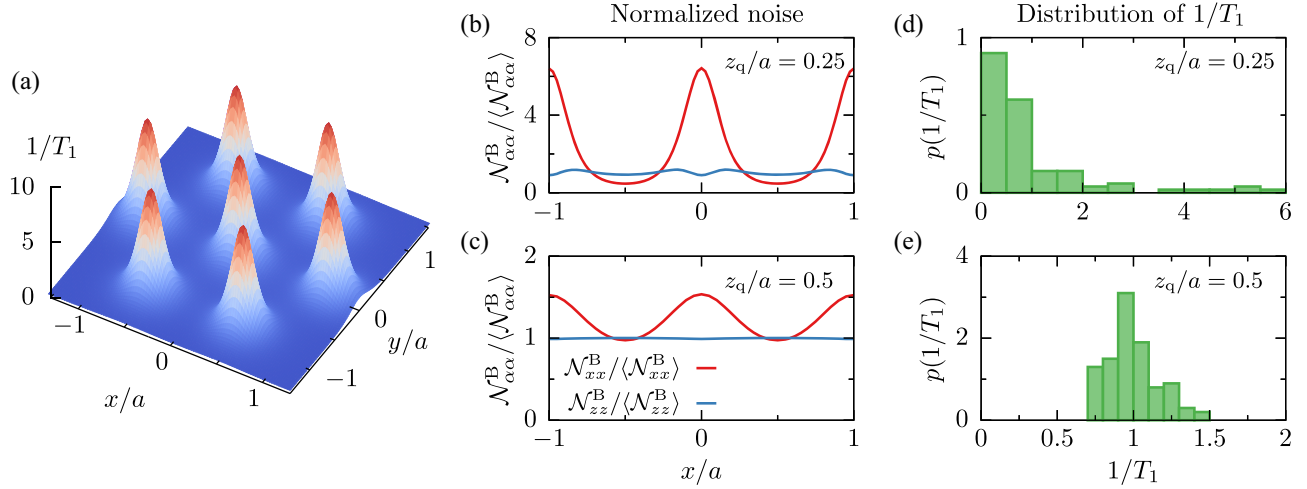


FIG. 1. Single-site resolution (SSR) of the WC with local magnetic noise spectroscopy. (a) Spatial dependence of the  $1/T_1$  relaxation rate of the qubit probe showing that the magnetic noise is strongly enhanced when the qubit is placed on top of an electron site. Here, we fixed  $z_q = 0.25a$ , the qubit quantization axis is aligned with  $\hat{z}$ , and we used the phonon Green’s function of the clean WC [44]. Panels (b) and (c) represent cuts of  $\mathcal{N}_{xx}^B$  and  $\mathcal{N}_{zz}^B$  along one of the edges in the triangular WC, showing that (i) the local magnetic noise is strongly anisotropic and (ii) when the probe is further away from the sample, the noise is more homogeneous. This is further illustrated in panels (d) and (e), where the broad distribution of  $1/T_1$  at  $z_q = 0.25a$  (d) becomes notably narrower at  $z_q = 0.5a$  (e). Various quantities are normalized by their spatial averages,  $\langle \dots \rangle$ , to highlight the magnitude of spatial fluctuations in the SSR regime.

SSR regime: (i) strong spatial inhomogeneity, (ii) anisotropy of the noise tensor, and (iii) broad distribution of qubit relaxation rates from different points in the plane. These characteristic features become weaker upon increasing the qubit-sample distance  $z_q$  [Figs. 1(c) and 1(e)]. The anisotropy of the noise near an electron site can be understood from the fact that an oscillating dipole in the plane would emit primarily in the direction perpendicular to the plane.

In the opposite limit  $z_q \gtrsim a$ , the noise (4) is well approximated by keeping only the  $\mathbf{G} = 0$  terms,

$$\mathcal{N}_{zz}^B(\omega) \approx \frac{\pi T n e^2 \omega}{c^2 z_q^2} \int_0^\infty dx x e^{-x} \text{Im} \left[ D_T \left( \frac{x}{2z_q}, \omega \right) \right], \quad (5)$$

i.e., the noise becomes independent of the in-plane position  $\mathbf{r}$ . For  $qa \ll 1$  and  $(\omega z_q/c)^2 \ll 1$ , one can approximate  $\mathcal{N}_{\alpha\beta}^B(\omega) \approx \text{diag}[\mathcal{N}_{zz}^B(\omega)/2, \mathcal{N}_{zz}^B(\omega)/2, \mathcal{N}_{zz}^B(\omega)]$ , implying there is only one independent component of the noise tensor [44]. In the same limit, the phonon Green’s function may be decomposed into transverse (T) and longitudinal (L) parts [47]. We observe that  $\mathcal{N}_{zz}^B(\omega)$  is determined by the transverse phonon Green’s function,  $D_T$ , which encodes the transverse sound mode. The existence of this mode captures the hallmark feature of the crystal phase—its rigidity to shear. For a clean WC, the dispersion of the transverse mode is  $\omega_T(\mathbf{q}) \approx v_s q$  for  $qa \ll 1$ .

Any realistic 2DEG system is affected by inhomogeneities of the sample. Here, we have implicitly assumed such disorder effects are not strong enough to completely destroy the local crystalline order [72]. While leaving

the crystal intact, weak disorder nevertheless has important effects on the phonon spectrum at larger length scales, relevant when  $z_q \gg a$ . The most significant effect is the “pinning” of the crystal, which opens a (pseudo) gap in the phonon spectrum:  $\omega_\lambda(q) \rightarrow \omega_0$  as  $q \rightarrow 0$  [73], leading to the emergence of a finite frequency “pinning” resonance,  $\omega_{\text{pin}}$ , in the absorption spectrum [48–50,74,75]. In the absence of an applied magnetic field,  $\omega_{\text{pin}} = \omega_0$ ; in a large out-of-plane magnetic field,  $\omega_{\text{pin}} = \omega_0^2/\omega_c$ , where  $\omega_c = eB/mc$  is the cyclotron frequency [76].

The pinning frequency defines an important characteristic length scale according to  $\omega_0 \sim v_s/R_c$ , where  $R_c$  is known as the “Larkin length” [77,78]. The Larkin length, assumed to satisfy  $R_c \gg a$ , is the length scale at which electrons “feel” the stochastic aspects of the disorder potential and metastability can manifest. Specifically, it is the length scale at which relative phonon displacements become of the order of a relevant microscopic length,  $\xi_0$ , which may correspond to the width of the electronic wave function localized to the WC lattice sites, the correlation length of the disorder potential, or the magnetic length in cases with a large perpendicular magnetic field. The various important length scales are summarized in Fig. 2.

Weak disorder also gives rise to broadening of the otherwise long-lived phonon modes. The foregoing discussion motivates the following simple parametrization of the phonon Green’s function in the regime  $qa \ll 1$ :

$$D_T(q, \omega) = -\frac{1}{m} \frac{1}{\omega^2 + 2i\gamma\omega - (v_s^2 q^2 + \omega_0^2)}, \quad (6)$$

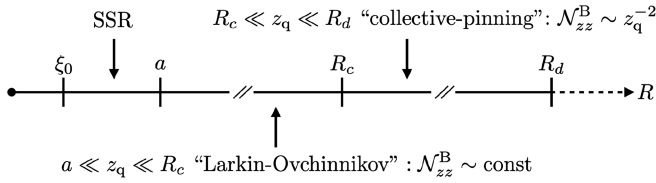


FIG. 2. Hierarchy of the relevant length scales for a weakly disordered WC. For  $R_d \gg R_c$ , topological defects become important.

where  $\gamma \sim \omega_0$  is the damping rate. Here, we have assumed that the length scales being probed are sufficiently long that the relevant observables are self-averaging, and translation invariance is effectively restored, implying in-plane momentum  $\mathbf{q}$  is a good quantum number [79]. This phenomenological form of the Green's function is in agreement with the results of more detailed calculations [44].

Utilizing the form of the Green's function (6), Eq. (5) for the noise becomes

$$\mathcal{N}_{zz}^B(\omega) = [\mathcal{N}_{zz}^B]_{\text{Liq}} \frac{1}{\tau\omega_0} \int_0^\infty dx x e^{-x} \times \frac{2\hat{\gamma}\hat{\omega}^2}{\{\hat{\omega}^2 - [\hat{\omega}_T^2(x/2z_q) + 1]\}^2 + 4\hat{\gamma}^2\hat{\omega}^2}, \quad (7)$$

where  $\hat{\omega} = \omega/\omega_0$  and  $\hat{\gamma} = \gamma/\omega_0$ . For the reference noise, we used the Johnson-Nyquist noise in the metallic phase  $[\mathcal{N}_{zz}^B]_{\text{Liq}} = \pi T \sigma_0 / (c^2 z_q^2)$ , where  $\sigma_0 = ne^2 \tau / m$  is the Drude conductivity and  $\tau$  is the scattering time. While the liquid state noise  $[\mathcal{N}_{zz}^B]_{\text{Liq}}$  is essentially featureless as a function of  $\omega$  and  $z_q$ , the noise in the WC phase exhibits a much richer structure. An immediate conclusion from Eq. (7) is that the low-frequency magnetic noise in the WC phase is significantly suppressed relative to that of the liquid:  $\mathcal{N}_{zz}^B \sim [\mathcal{N}_{zz}^B]_{\text{Liq}} \times (\omega/\omega_0)^2$  as  $\omega \rightarrow 0$ , yielding a crude signature of the transition from the metallic to insulating phase [80]. For an estimate of the liquid-state noise near the WC transition, we consider a TMD system at  $T \sim 10$  K,  $z_q \sim 10$  nm, and  $n \sim 10^{11} \text{ cm}^{-2}$ , and use the mobilities reported in Ref. [51]. This yields  $[\mathcal{N}_{zz}^B]_{\text{Liq}} \sim 5 \text{ pT}^2 \times \text{Hz}^{-1}$ , which is within the sensitivity of current qubit sensors [15,20]. For bilayer WCs, the noise will be further enhanced; for TMD bilayers specifically, we find  $[\mathcal{N}_{zz}^B]_{\text{Liq}} \sim 200 \text{ pT}^2 \times \text{Hz}^{-1}$  [44]. We thus expect detection of the WC transition with noise sensing, via both  $1/T_1$  and  $1/T_2$  measurements, is within experimental reach.

More refined information may be extracted by considering how the noise varies with the probe frequency  $\omega$  and height  $z_q$ . As shown in Fig. 3, there is a resonant enhancement for  $\omega \approx \sqrt{v_s^2 q_*^2 + \omega_0^2}$ , where the wave vector is determined by the probe height,  $q_* = 1/2z_q$ . The peak position moves closer to the phonon dispersion as the

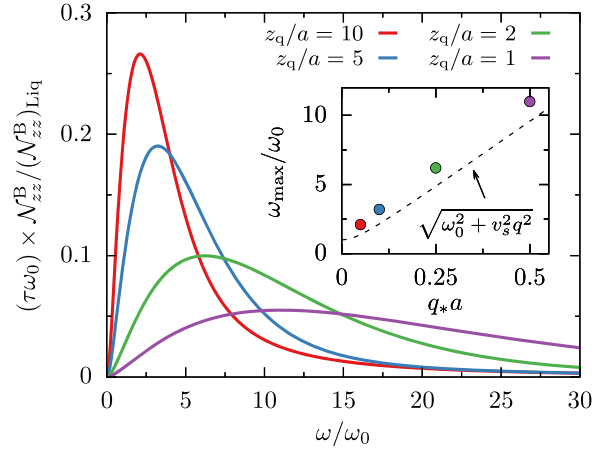


FIG. 3. Collective behavior in the WC. Magnetic noise as a function of  $\omega$  for various probe heights  $z_q$  shows an enhancement upon crossing the transverse phonon frequency  $\omega = \omega_T(q_*)$  at  $q_* = 1/2z_q$ . Inset: tracking the maxima of  $\mathcal{N}_{zz}^B(\omega)$  for various  $z_q$  enables reconstructing the dispersion curve  $\omega_T(q)$ .

phonons become sharper, i.e., as the disorder effects become weaker. Thus, for a sufficiently clean WC corresponding to  $\omega_0 \ll \omega_p$ , mapping of the magnetic noise in the  $(z_q, \omega)$  space allows for direct extraction of the transverse phonon dispersion curve. Even if stronger disorder precludes such mapping, at large enough probe heights the noise still exhibits a resonant enhancement at  $\omega_0$ . Similarly, we anticipate that other  $q = 0$  resonances unique to WC phases can be studied with the noise measurements. One notable example is the optical phonon in bilayer WCs, corresponding to out-of-phase charge oscillations between the layers. Without disorder, the qubit probe separated farther than the interlayer spacing averages over the layers and is insensitive to the optical mode. With disorder, however, differences in pinning between the layers will couple the optical mode into the layer-averaged response [44] [Fig. 4]. We note that other interesting optical modes have also been recently predicted for WCs in multivalley 2DEGs [81].

Experimental feasibility of mapping the phonon spectrum requires an estimate of the pinning frequency  $\omega_0$ . This frequency is determined by the disorder of the sample, making a direct evaluation from microscopic considerations challenging. However, if we assume the disorder effects are relatively weak, as evidenced by the appreciable WC correlation length inferred from experiments [2], then it is reasonable to assume  $\omega_0 \lesssim \omega_p$ . To be within the operating regime of nitrogen-vacancy or silicon-vacancy centers [69,70], one requires  $\omega_0 \lesssim 50$  GHz (Fig. 3). Finite temperature effects should help push  $\omega_0$  into the experimentally accessible range, as phonon frequencies are expected to soften upon approaching the thermal melting transition. Fabrication of cleaner TMD samples will also both increase the overall noise and decrease  $\omega_0$ .

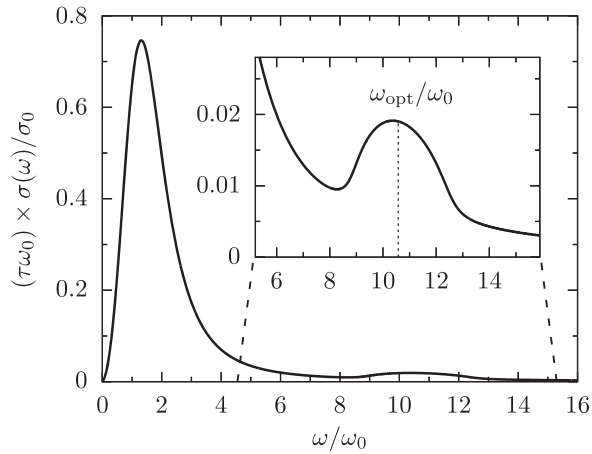


FIG. 4. Conductivity in the bilayer WC exhibits an additional peak at the optical phonon frequency, which couples to the noise sensor due to the presence of a weak disorder.

Application of a large perpendicular magnetic field [82] shifts the pinning resonance to a lower frequency and makes it narrower [48,49,75]. All these effects increase the feasibility of our proposal.

In the short distance SSR regime, in addition to the direct imaging of the WC lattice one could potentially extract a number of important properties relating to the nano and mesoscale properties of the system. This would be particularly useful to study the physics near quantum melting of the WC, where there have been proposals of intermediate phases involving mesoscale inhomogeneity and other forms of symmetry breaking such as nematicity [83,84]. In the regime of a far-separated sensor, monitoring the evolution of the phonon spectrum upon increasing electron density would shed light on quantum effects in the WC. Some interesting questions in this regard include the extent to which magnetic tendencies of the WC are encoded in the elastic coefficients of the crystal and the role of phonon softening for melting. Although we have not explored it in detail here, the spin properties of the WC, which are expected to be particularly rich near melting [85,86], can also be probed via magnetic noise sensing. Beyond WCs, we also expect the techniques described here to be useful in studying moiré systems, which have a similarly large emergent length scale associated with the moiré unit cell.

The authors would like to thank E. Kaxiras, A. Barr, A. Imamoglu, P. Volkov, C. Kuhlenkamp, R. Xue, J. Curtis, Z. Sun, M. Fogler, V. Fal'ko, R. Citro, A. Yacoby, and K. Agarwal for fruitful discussions. The work of P. E. D. was sponsored by the Army Research Office and was accomplished under Grant No. W911NF-21-1-0184. I. E. acknowledges support from the AFOSR Grant No. FA9550-21-1-0216 and the University of Wisconsin–Madison. E. D. acknowledges support from the SNSF Project

No. 200021\_212899. T. G. acknowledges support from the SNSF Projects No. 200020\_188687 and No. 200020-219400. M. D. L. and A. A. Z. were supported by the NSF and CUA.

\*These authors contributed equally to this letter.

- [1] E. Wigner, On the interaction of electrons in metals, *Phys. Rev.* **46**, 1002 (1934).
- [2] T. Smoleński, P. E. Dolgirev, C. Kuhlenkamp, A. Popert, Y. Shimazaki, P. Back, X. Lu, M. Kroner, K. Watanabe, T. Taniguchi, I. Esterlis, E. Demler, and A. Imamoglu, Signatures of Wigner crystal of electrons in a monolayer semiconductor, *Nature (London)* **595**, 53 (2021).
- [3] Y. Zhou, J. Sung, E. Brutschea, I. Esterlis, Y. Wang, G. Scuri, R. J. Gelly, H. Heo, T. Taniguchi, K. Watanabe, G. Zaránd, M. D. Lukin, P. Kim, E. Demler, and H. Park, Bilayer Wigner crystals in a transition metal dichalcogenide heterostructure, *Nature (London)* **595**, 48 (2021).
- [4] M. S. Hossain, M. Ma, K. Rosales, Y. Chung, L. Pfeiffer, K. West, K. Baldwin, and M. Shayegan, Observation of spontaneous ferromagnetism in a two-dimensional electron system, *Proc. Natl. Acad. Sci. U.S.A.* **117**, 32244 (2020).
- [5] M. S. Hossain, M. K. Ma, K. A. Villegas-Rosales, Y. J. Chung, L. N. Pfeiffer, K. W. West, K. W. Baldwin, and M. Shayegan, Spontaneous valley polarization of itinerant electrons, *Phys. Rev. Lett.* **127**, 116601 (2021).
- [6] J. Falson, I. Sodemann, B. Skinner, D. Tabrea, Y. Kozuka, A. Tsukazaki, M. Kawasaki, K. von Klitzing, and J. H. Smet, Competing correlated states around the zero-field Wigner crystallization transition of electrons in two dimensions, *Nat. Mater.* **21**, 311 (2022).
- [7] A notable new probe is the STM imaging technique developed in [8].
- [8] H. Li, S. Li, E. C. Regan, D. Wang, W. Zhao, S. Kahn, K. Yumigeta, M. Blei, T. Taniguchi, K. Watanabe *et al.*, Imaging two-dimensional generalized Wigner crystals, *Nature (London)* **597**, 650 (2021).
- [9] I. V. Kukushkin, V. I. Fal'ko, R. J. Haug, K. Von Klitzing, K. Eberl, and K. Töttemayer, Evidence of the triangular lattice of crystallized electrons from time resolved luminescence, *Phys. Rev. Lett.* **72**, 3594 (1994).
- [10] X. Cui, G.-H. Lee, Y. D. Kim, G. Arefe, P. Y. Huang, C.-H. Lee, D. A. Chenet, X. Zhang, L. Wang, F. Ye *et al.*, Multi-terminal transport measurements of MoS<sub>2</sub> using a van der Waals heterostructure device platform, *Nat. Nanotechnol.* **10**, 534 (2015).
- [11] X. Cui, E.-M. Shih, L. A. Jauregui, S. H. Chae, Y. D. Kim, B. Li, D. Seo, K. Pistunova, J. Yin, J.-H. Park *et al.*, Low-temperature ohmic contact to monolayer MoS<sub>2</sub> by van der Waals bonded Co/h-BN electrodes, *Nano Lett.* **17**, 4781 (2017).
- [12] S. Hong, M. S. Grinolds, L. M. Pham, D. Le Sage, L. Luan, R. L. Walsworth, and A. Yacoby, Nanoscale magnetometry with NV centers in diamond, *MRS Bull.* **38**, 155 (2013).
- [13] M. S. Grinolds, S. Hong, P. Maletinsky, L. Luan, M. D. Lukin, R. L. Walsworth, and A. Yacoby, Nanoscale magnetic imaging of a single electron spin under ambient conditions, *Nat. Phys.* **9**, 215 (2013).

- [14] L. Rondin, J.-P. Tetienne, T. Hingant, J.-F. Roch, P. Maletinsky, and V. Jacques, Magnetometry with nitrogen-vacancy defects in diamond, *Rep. Prog. Phys.* **77**, 056503 (2014).
- [15] B. J. Shields, Q. P. Unterreithmeier, N. P. de Leon, H. Park, and M. D. Lukin, Efficient readout of a single spin state in diamond via spin-to-charge conversion, *Phys. Rev. Lett.* **114**, 136402 (2015).
- [16] S. Kolkowitz, A. Safira, A. High, R. Devlin, S. Choi, Q. Unterreithmeier, D. Patterson, A. Zibrov, V. Manucharyan, H. Park *et al.*, Probing Johnson noise and ballistic transport in normal metals with a single-spin qubit, *Science* **347**, 1129 (2015).
- [17] Y. Dovzhenko, F. Casola, S. Schlotter, T. Zhou, F. Büttner, R. Walsworth, G. Beach, and A. Yacoby, Magnetostatic twists in room-temperature skyrmions explored by nitrogen-vacancy center spin texture reconstruction, *Nat. Commun.* **9**, 2712 (2018).
- [18] F. Casola, T. Van Der Sar, and A. Yacoby, Probing condensed matter physics with magnetometry based on nitrogen-vacancy centres in diamond, *Nat. Rev. Mater.* **3**, 1 (2018).
- [19] S. Hsieh, P. Bhattacharyya, C. Zu, T. Mittiga, T. Smart, F. Machado, B. Kobrin, T. Höhn, N. Rui, M. Kamrani *et al.*, Imaging stress and magnetism at high pressures using a nanoscale quantum sensor, *Science* **366**, 1349 (2019).
- [20] T. I. Andersen, B. L. Dwyer, J. D. Sanchez-Yamagishi, J. F. Rodriguez-Nieva, K. Agarwal, K. Watanabe, T. Taniguchi, E. A. Demler, P. Kim, H. Park *et al.*, Electron-phonon instability in graphene revealed by global and local noise probes, *Science* **364**, 154 (2019).
- [21] L. Thiel, Z. Wang, M. A. Tschudin, D. Rohner, I. Gutiérrez-Lezama, N. Ubrig, M. Gibertini, E. Giannini, A. F. Morpurgo, and P. Maletinsky, Probing magnetism in 2d materials at the nanoscale with single-spin microscopy, *Science* **364**, 973 (2019).
- [22] A. Rustagi, I. Bertelli, T. Van Der Sar, and P. Upadhyaya, Sensing chiral magnetic noise via quantum impurity relaxation, *Phys. Rev. B* **102**, 220403(R) (2020).
- [23] A. Chatterjee, P. Stevenson, S. De Franceschi, A. Morello, N. P. de Leon, and F. Kuemmeth, Semiconductor qubits in practice, *Nat. Rev. Phys.* **3**, 157 (2021).
- [24] T. X. Zhou, J. J. Carmiggelt, L. M. Gächter, I. Esterlis, D. Sels, R. J. Stöhr, C. Du, D. Fernandez, J. F. Rodriguez-Nieva, F. Büttner *et al.*, A magnon scattering platform, *Proc. Natl. Acad. Sci. U.S.A.* **118**, e2019473118 (2021).
- [25] X.-Y. Zhang, Y.-X. Wang, T. A. Tartaglia, T. Ding, M. J. Gray, K. S. Burch, F. Tafti, and B. B. Zhou, ac susceptometry of 2D van der Waals magnets enabled by the coherent control of quantum sensors, *PRX Quantum* **2**, 030352 (2021).
- [26] H. Wang, S. Zhang, N. J. McLaughlin, B. Flebus, M. Huang, Y. Xiao, C. Liu, M. Wu, E. E. Fullerton, Y. Tserkovnyak *et al.*, Noninvasive measurements of spin transport properties of an antiferromagnetic insulator, *Sci. Adv.* **8**, eabg8562 (2022).
- [27] Y.-X. Wang, X.-Y. Zhang, C. Li, X. Yao, R. Duan, T. K. Graham, Z. Liu, F. Tafti, D. Broido, Y. Ran *et al.*, Visualization of bulk and edge photocurrent flow in anisotropic Weyl semimetals, *Nat. Phys.* **19**, 507 (2023).
- [28] A. Gottscholl, M. Diez, V. Soltamov, C. Kasper, A. Sperlich, M. Kianinia, C. Bradac, I. Aharonovich, and V. Dyakonov, Room temperature coherent control of spin defects in hexagonal boron nitride, *Sci. Adv.* **7**, eabf3630 (2021).
- [29] A. Gottscholl, M. Diez, V. Soltamov, C. Kasper, D. Krauß, A. Sperlich, M. Kianinia, C. Bradac, I. Aharonovich, and V. Dyakonov, Spin defects in HBN as promising temperature, pressure and magnetic field quantum sensors, *Nat. Commun.* **12**, 4480 (2021).
- [30] S. Castelletto and A. Boretti, Color centers in wide-bandgap semiconductors for subdiffraction imaging: A review, *Adv. Opt. Photonics* **3**, 054001 (2021).
- [31] M. Huang, J. Zhou, D. Chen, H. Lu, N. J. McLaughlin, S. Li, M. Alghamdi, D. Djugba, J. Shi, H. Wang *et al.*, Wide field imaging of van der Waals ferromagnet Fe<sub>3</sub>GeTe<sub>2</sub> by spin defects in hexagonal boron nitride, *Nat. Commun.* **13**, 5369 (2022).
- [32] S. Vaidya, X. Gao, S. Dikshit, I. Aharonovich, and T. Li, Quantum sensing and imaging with spin defects in hexagonal boron nitride, *Adv. Phys.* **8**, 2206049 (2023).
- [33] A. Healey, S. Scholten, T. Yang, J. Scott, G. Abrahams, I. Robertson, X. Hou, Y. Guo, S. Rahman, Y. Lu *et al.*, Quantum microscopy with van der Waals heterostructures, *Nat. Phys.* **19**, 87 (2023).
- [34] D. A. Bonnell, D. N. Basov, M. Bode, U. Diebold, S. V. Kalinin, V. Madhavan, L. Novotny, M. Salmeron, U. D. Schwarz, and P. S. Weiss, Imaging physical phenomena with local probes: From electrons to photons, *Rev. Mod. Phys.* **84**, 1343 (2012).
- [35] B.-Y. Jiang, L. Zhang, A. Castro Neto, D. Basov, and M. Fogler, Generalized spectral method for near-field optical microscopy, *J. Appl. Phys.* **119**, 054305 (2016).
- [36] F. Dolde, M. W. Doherty, J. Michl, I. Jakobi, B. Naydenov, S. Pezzagna, J. Meijer, P. Neumann, F. Jelezko, N. B. Manson *et al.*, Nanoscale detection of a single fundamental charge in ambient conditions using the NV<sup>-</sup> center in diamond, *Phys. Rev. Lett.* **112**, 097603 (2014).
- [37] B. A. Myers, A. Ariyaratne, and A. B. Jayich, Double-quantum spin-relaxation limits to coherence of near-surface nitrogen-vacancy centers, *Phys. Rev. Lett.* **118**, 197201 (2017).
- [38] G. Wolfowicz, S. Whiteley, and D. Awschalom, Electrometry by optical charge conversion of deep defects in 4h-SiC, *Proc. Natl. Acad. Sci. U.S.A.* **115**, 7879 (2018).
- [39] B. Yang, T. Murooka, K. Mizuno, K. Kim, H. Kato, T. Makino, M. Ogura, S. Yamasaki, M. E. Schmidt, H. Mizuta *et al.*, Vector electrometry in a wide-gap-semiconductor device using a spin-ensemble quantum sensor, *Phys. Rev. Appl.* **14**, 044049 (2020).
- [40] K. Bian, W. Zheng, X. Zeng, X. Chen, R. Stöhr, A. Denisenko, S. Yang, J. Wrachtrup, and Y. Jiang, Nanoscale electric-field imaging based on a quantum sensor and its charge-state control under ambient condition, *Nat. Commun.* **12**, 2457 (2021).
- [41] Z. Qiu, A. Hamo, U. Vool, T. X. Zhou, and A. Yacoby, Nanoscale electric field imaging with an ambient scanning quantum sensor microscope, *npj Quantum Inf.* **8**, 107 (2022).
- [42] L. S. Langsjoen, A. Poudel, M. G. Vavilov, and R. Joynt, Qubit relaxation from evanescent-wave Johnson noise, *Phys. Rev. A* **86**, 010301(R) (2012).

- [43] As a concrete example, in the case of a nitrogen-vacancy center, the dynamic magnetic noise would, depending on the direction of magnetic field, cause transitions between the states with  $m_s = 0$  and  $m_s = \pm 1$ , or lead to fluctuations of energy differences between states with different  $m_s$  causing the 2018 probing. In [44], we also analyze the electrical noise that can cause transitions between  $m_s = -1$  and  $m_s = +1$ , resulting in energy difference fluctuations between the states with  $m_s = 0$  and  $|m_s| = 1$  and, thus, affecting  $1/T_2$ -like measurements [37].
- [44] See Supplemental Material at <http://link.aps.org/supplemental/10.1103/PhysRevLett.132.246504> for additional theoretical details. The discussion there includes (i) the relation between optical conductivity and phonon Green's function, (ii) single-site resolution with local noise spectroscopy, (iii) magnetic noise and (iv) electric noise calculations for systems without time-reversal symmetry, (v) phonon dispersion of a clean bilayer WC, and (vi) Gaussian variational approach to treat disorder effects in bilayer WCs. The Supplemental Material includes Refs. [3,19,36,42,45–59].
- [45] K. Agarwal, R. Schmidt, B. Halperin, V. Oganesyan, G. Zaránd, M. D. Lukin, and E. Demler, Magnetic noise spectroscopy as a probe of local electronic correlations in two-dimensional systems, *Phys. Rev. B* **95**, 155107 (2017).
- [46] F. Machado, E. A. Demler, N. Y. Yao, and S. Chatterjee, Quantum noise spectroscopy of dynamical critical phenomena, *Phys. Rev. Lett.* **131**, 070801 (2023).
- [47] L. Bonsall and A. Maradudin, Some static and dynamical properties of a two-dimensional Wigner crystal, *Phys. Rev. B* **15**, 1959 (1977).
- [48] R. Chitra, T. Giamarchi, and P. Le Doussal, Dynamical properties of the pinned Wigner crystal, *Phys. Rev. Lett.* **80**, 3827 (1998).
- [49] R. Chitra, T. Giamarchi, and P. Le Doussal, Pinned Wigner crystals, *Phys. Rev. B* **65**, 035312 (2001).
- [50] R. Chitra and T. Giamarchi, Zero field Wigner crystal, *Eur. Phys. J. B* **44**, 455 (2005).
- [51] S. Larentis, H. C. P. Movva, B. Fallahzad, K. Kim, A. Behroozi, T. Taniguchi, K. Watanabe, S. K. Banerjee, and E. Tutuc, Large effective mass and interaction-enhanced Zeeman splitting of  $k$ -valley electrons in  $\text{MoSe}_2$ , *Phys. Rev. B* **97**, 201407(R) (2018).
- [52] H. Fukuyama and P. A. Lee, Pinning and conductivity of two-dimensional charge-density waves in magnetic fields, *Phys. Rev. B* **18**, 6245 (1978).
- [53] G. Goldoni and F. M. Peeters, Stability, dynamical properties, and melting of a classical bilayer Wigner crystal, *Phys. Rev. B* **53**, 4591 (1996).
- [54] A. Abragam, *The Principles of Nuclear Magnetism* (Oxford University Press, New York, 1961), Vol. 32.
- [55] B. Spivak, S. V. Kravchenko, S. A. Kivelson, and X. P. A. Gao, Colloquium: Transport in strongly correlated two dimensional electron fluids, *Rev. Mod. Phys.* **82**, 1743 (2010).
- [56] P. Rodriguez-Lopez, W. J. M. Kort-Kamp, D. A. R. Dalvit, and L. M. Woods, Nonlocal optical response in topological phase transitions in the graphene family, *Phys. Rev. Mater.* **2**, 014003 (2018).
- [57] T. Giamarchi and P. Le Doussal, Elastic theory of flux lattices in the presence of weak disorder, *Phys. Rev. B* **52**, 1242 (1995).
- [58] T. Giamarchi and P. Le Doussal, Variational theory of elastic manifolds with correlated disorder and localization of interacting quantum particles, *Phys. Rev. B* **53**, 15206 (1996).
- [59] M. Mézard and G. Parisi, Replica field theory for random manifolds, *J. Phys. I (France)* **1**, 809 (1991).
- [60] J. F. Rodriguez-Nieva, K. Agarwal, T. Giamarchi, B. I. Halperin, M. D. Lukin, and E. Demler, Probing one-dimensional systems via noise magnetometry with single spin qubits, *Phys. Rev. B* **98**, 195433 (2018).
- [61] B. Flebus and Y. Tserkovnyak, Quantum-impurity relaxation of magnetization dynamics, *Phys. Rev. Lett.* **121**, 187204 (2018).
- [62] S. Chatterjee, J. F. Rodriguez-Nieva, and E. Demler, Diagnosing phases of magnetic insulators via noise magnetometry with spin qubits, *Phys. Rev. B* **99**, 104425 (2019).
- [63] P. E. Dolgirev, S. Chatterjee, I. Esterlis, A. A. Zibrov, M. D. Lukin, N. Y. Yao, and E. Demler, Characterizing two-dimensional superconductivity via nanoscale noise magnetometry with single-spin qubits, *Phys. Rev. B* **105**, 024507 (2022).
- [64] S. Chatterjee, P. E. Dolgirev, I. Esterlis, A. A. Zibrov, M. D. Lukin, N. Y. Yao, and E. Demler, Single-spin qubit magnetic spectroscopy of two-dimensional superconductivity, *Phys. Rev. Res.* **4**, L012001 (2022).
- [65] We remark that a distinct but related proposal, regarding spatially inhomogeneous noise near an isolated impurity, was made in Ref. [45].
- [66] Y. Yu, C. Yang, M. Baggioli, A. E. Phillips, A. Zaccane, L. Zhang, R. Kajimoto, M. Nakamura, D. Yu, and L. Hong, The  $\omega^3$  scaling of the vibrational density of states in quasi-2d nanoconfined solids, *Nat. Commun.* **13**, 3649 (2022).
- [67] X. Guo, A. M. Stramma, Z. Li, W. G. Roth, B. Huang, Y. Jin, R. A. Parker, J. A. Martínez, N. Shofer, C. P. Michaels *et al.*, Microwave-based quantum control and coherence protection of tin-vacancy spin qubits in a strain-tuned diamond membrane heterostructure, *Phys. Rev. X* **13**, 041037 (2023).
- [68] T. Cocker, V. Jelic, R. Hillenbrand, and F. Hegmann, Nanoscale terahertz scanning probe microscopy, *Nat. Photonics* **15**, 558 (2021).
- [69] M. Ludovic and D. Thierry, Nitrogen-vacancy centers in diamond for instantaneous spectral analysis in the radio-frequency domain up to 18 GHz, in *Proceedings of the 2018 International Topical Meeting on Microwave Photonics (MWP)* (IEEE, New York, 2018), pp. 1–4.
- [70] G. Wang, Y.-X. Liu, J. M. Schloss, S. T. Alsld, D. A. Braje, and P. Cappellaro *et al.*, Sensing of arbitrary-frequency fields using a quantum mixer, *Phys. Rev. X* **12**, 021061 (2022).
- [71] S. Brem and E. Malic, Terahertz fingerprint of monolayer Wigner crystals, *Nano Lett.* **22**, 1311 (2022).
- [72] In this regard, the SSR method would allow one to image the distorted lattice giving access to the average displacements due to disorder and long-range crystalline correlations.
- [73] To be more precise, weak disorder gives rise to a distribution of gap frequencies, which manifests as an imaginary

- (frequency-dependent) correction to the  $\omega_0$  pole in the phonon propagator [44].
- [74] H. Fukuyama and P. A. Lee, Dynamics of the charge-density wave. I. Impurity pinning in a single chain, *Phys. Rev. B* **17**, 535 (1978).
- [75] M. M. Fogler and D. A. Huse, Dynamical response of a pinned two-dimensional Wigner crystal, *Phys. Rev. B* **62**, 7553 (2000).
- [76] We note that, to experimentally access the SSR regime, the suppression of low-energy density of states  $g(\omega)$  due to development of the pinning (pseudo) gap will likely further experimentally constrain  $\omega \gtrsim \omega_0$ .
- [77] A. I. Larkin, Effect of inhomogeneties on the structure of the mixed state of superconductors, *ZhETF* **58**, 1466 (1970) [**31**, 784 (1970)].
- [78] A. Larkin and Y. N. Ovchinnikov, Pinning in type II superconductors, *J. Low Temp. Phys.* **34**, 409 (1979).
- [79] Strictly speaking, this analysis should be valid for  $z_q \gtrsim R_c$ . For a more quantitative understanding of the regime  $a \lesssim z_q \lesssim R_c$ , a different treatment of disorder effects might be required. In this regime, the probe is close enough to the sample so that there is no self-averaging yet, while, at the same time, the local properties are important. One implication could be that in this regime, one should use the form as in Eq. (6), except with much smaller linewidth  $\gamma$ , which is expected to make the magnetic noise larger. We leave careful analysis of this regime to future work.
- [80] We remark the precise power law of the noise at low frequencies is still an open question requiring a more sophisticated treatment. Despite this theoretical uncertainty, one might nevertheless attempt to do generalized echolike measurements, in particular, analogs of the Carr-Purcell-Meiboom-Gill pulse sequence [46], as they can give direct experimental access to the scaling of the noise with frequency.
- [81] V. Calvera, S. A. Kivelson, and E. Berg, Pseudo-spin order of Wigner crystals in multi-valley electron gases, [arXiv: 2210.09326](https://arxiv.org/abs/2210.09326).
- [82] In [44], we analyse the noise for the case of systems without time-reversal symmetry, such as those in a magnetic field.
- [83] B. Spivak and S. A. Kivelson, Phases intermediate between a two-dimensional electron liquid and Wigner crystal, *Phys. Rev. B* **70**, 155114 (2004).
- [84] R. Jamei, S. Kivelson, and B. Spivak, Universal aspects of Coulomb-frustrated phase separation, *Phys. Rev. Lett.* **94**, 056805 (2005).
- [85] S. Chakravarty, S. Kivelson, C. Nayak, and K. Voelker, Wigner glass, spin liquids and the metal-insulator transition, *Philos. Mag. B* **79**, 859 (1999).
- [86] K.-S. Kim, C. Murthy, A. Pandey, and S. A. Kivelson, Interstitial-induced ferromagnetism in a two-dimensional Wigner crystal, *Phys. Rev. Lett.* **129**, 227202 (2022).